SCIENTIFIC REPORTS

OPEN

SUBJECT AREAS:
BIOSENSORS
CANCER IMAGING
BIOMATERIALS
BIOMARKERS

Received
19 December 2013

Accepted
20 February 2014

Published
17 March 2014

Correspondence and requests for materials should be addressed to X.M.W. (xuewang@seu.edu.cn)

Near-infrared fluorescence imaging of cancer cells and tumors through specific biosynthesis of silver nanoclusters

Shengping Gao[1], Donghua Chen[1], Qiwei Li[1], Jing Ye[1], Hui Jiang[1], Christian Amatore[2] & Xuemei Wang[1]

[1]State Key Laboratory of Bioelectronics (Chien-Shiung Wu Lab), School of Biological Science and Medical Engineering, Southeast University, Nanjing, 210096, China, [2]Ecole Normale Supérieure, UMR CNRS-ENS-UPMC 8640 and LIA CNRS XiamENS NanoBioChem Departement de Chimie, 24 rue Lhomond 75005 Paris (France).

Human life toll by cancer, one of the highest among most dreaded diseases in advanced societies, could be reduced by implementing evidence-based strategies for its prevention, early diagnosis and assessment of the progress and suitability of therapies by fast and non-invasive methods. In this contribution, a novel strategy is reported for highly sensitive recognition and in vivo imaging of cancer cells taking advantage of their spontaneous ability to generate silver nanoclusters (NCs) with high near-infrared fluorescence emission by intracellular reduction of innocuous silver salts. Both ex vivo experiments comparing cancer cell models to normal cells and in vivo imaging of subcutaneous xenografted tumor (cervical carcinoma model) in nude mice established the validity of this strategy for precise and selective imaging of cells and tumors. Furthermore, it was observed that the spontaneous self-generation of Ag NCs by tumors in their inside led to drastic reduction of their sizes and often to complete remission, thus providing important hope for new therapy strategies based on cheap and readily available agents.

At least in modern societies, cancer is one of the most dreaded diseases and still remains a major threat to human life. According to the World Health Organization, cancer accounted for 7.6 million deaths in 2008 (13% of all deaths), and this number is expected to rise to 13.1 million by 2030. Such high toll could be reduced and controlled by implementing evidence-based strategies for prevention and early detection of cancer. Many cancers have a high chance of cure if detected early and treated adequately, but too many patients are diagnosed in later or too advanced stage[1]. It is therefore imperative to improve cancer diagnostic methods in early or even pre-syndrome stages[2]. Near-infrared fluorescence (NIRF) imaging techniques have recently brought high promises in this respect. Compared to other imaging approaches[3], NIRF imaging based on target-selective probes has several major advantages including high sensitivity and specificity[4,5]. Fluorophores in the near-infrared (NIR) wavelength are of particular interest for in vivo imaging because tissue autofluorescence and light absorption in the NIR range (650 ~ 900 nm) are low, and NIR light can pass across several centimeters of heterogeneous living tissues[6]. In vivo optical imaging has a long history involving bioluminescent proteins[7], fluorescent proteins[8], and fluorescent dyes[9]. However, conventional fluorophores often suffer from small Stokes shifts, poor photostability, too fast photobleaching, aggregation and high plasma protein binding rates which are not fit for long-term imaging. Furthermore, usual strategies based on molecular fluorophores require that the fluorescent probe is linked to a ligand whose role is to recognize the target tissue[10]. Hence, these methods often suffer from a poor sensitivity due to the limited number of fluorophores conjugated per ligand[11]. In addition, long-term in vivo toxicities of the majority of fluorophores remain still to be evaluated[12].

For the resolution of these problems, attention has been channeled increasingly toward nanotechnology to search for new classes of more effective probes[13]. Many nanomaterials including some quantum dots or nanoclusters are already widely used as fluorescence probes[14]. Indeed, the optical and electronic properties of nanoclusters (NCs) are governed by the fact that their sub-nanometer dimensions are comparable to the Fermi wavelengths of conduction electrons, leading to molecule-like features such as discrete size-dependent fluorescence. Fluorescence of noble metal NCs consisting of several tens of atoms have thus attracted significant attention in the past decade owing to their remarkable optical properties[15]. Among the various metal nanoclusters reported to date[16], Ag-based ones are of special interest due to their ultrasmall size, biocompatibility, nontoxicity, good photostability and high NIR fluorescence[17]. Furthermore, Ag NCs generate large fluorescence intensities, often of an order of magnitude higher than traditional fluorophores[18]. In addition, the fluorescence of Ag NCs exhibits

greater photostability enabling sufficient long-term imaging. Another practical advantage of Ag NCs is that their excitation and emission spectra are narrow and symmetric, thus minimizing any overlapping of colors in multi-components imaging applications[19].

The unique properties of Ag NCs for biological imaging make them efficient for the detection of tumors at an early stage of their development in vivo. However, several important issues need to be resolved before this may happen. Among these, two crucial points are detrimental and need to be overcome: (i) imaging of tumors requires that Ag NCs administered to an animal are bound to specific ligands prone to target cancerous tissues; (ii) unless they are capped with adequate molecules able to elude the immune system, Ag NCs are excreted efficiently through renal clearance, thus decreasing their residence times in organisms after administration.

Herein, we wish to report a novel strategy for in situ self-imaging of cancer cells and tumors through their spontaneous ability to biosynthesize Ag NCs following their treatment with a specific Ag^+ derivative $[Ag(GSH)]^+$; see Experimental Section) and exogenous glutathione (GSH). GSH is a thiolated tripeptide present in normal eukaryote cells at rather high concentrations (ca 5 mM) and is responsible for maintaining the cellular redox homeostasis through its facile oxidation into glutathione disulfide (GSSG; see below). Cancerous cells exhibit higher GSH-GSSG concentrations compared to normal cells with a marked unbalance toward GSSG as a result of their efficient coping with the high productions of reactive oxygen (ROS) or nitrogen (RNS) species by cancer cells and tumors. On the other hand, thiols and disulfides are excellent ligands of silver surfaces on which they attach spontaneously to create self-assembled monolayers. Hence, glutathione complexation and reduction of Ag^+ ions into Ag NCs is expected to be higher in cancerous cells compared to normal ones[20], thus offering a possibility for selective self-imaging by cells.

In agreement with such views, this work establishes that the intracellular biosynthesis of Ag NCs by cancerous cells incubated with silver ions is spontaneous, while this does not occur in non-cancerous cells even after longer incubation times. The present observations demonstrate that such specific biosynthetic ability to generate Ag NCs from silver salts offers a promising strategy for highly sensitive and rapid in vivo self-imaging of cancer cells in a culture of living tumors ideal for biomedical applications requiring specific and sensitive diagnosis and imaging of tumors.

Results

Biosynthesis and characterization of Ag NCs. Ag NCs were spontaneously biosynthesized in situ by HeLa cancer cell (Shanghai Institutes for Biological Sciences, Chinese Academy of Sciences) models treated with a silver salt derivative $[Ag(GSH)]^+$, viz., resulting from the complexes of GSH and $AgNO_3$ as described in Experimental Section. The intracellular presence of the ensuring biosynthesized silver NCs was characterized by UV-vis absorption spectroscopy, fluorescence spectroscopy, transmission electron microscope (TEM), X-ray photoelectron spectroscopy (XPS), etc. These Ag NCs displayed NIRF emissions with excitation and emission wavelengths of 590 and 670 nm, respectively (Figure 1A). Interestingly, in situ biosynthesis of Ag NCs was not observed in non-cancerous control cells after even longer incubation times (Figure S1), which is consistent with our previous observations about the specificity of Au nanoclusters biosynthesis by cancer cells treated with gold salts ($HAuCl_4$)[16]. A typical TEM image of the resulting Ag NCs is provided in Figure 1Ba, evidencing their high monodispersity and uniform sizes of 1.1 ± 0.2 nm (Figure 1Bb). TEM also established that biosynthesized Ag NCs involved silver atoms planes with an interplane distance of ca. 0.1 nm, were almost spherical and had no noticeable trend to agglomerate. Such a narrow size distribution and the absence of agglomeration suggest that the intracellular reduction of silver ions

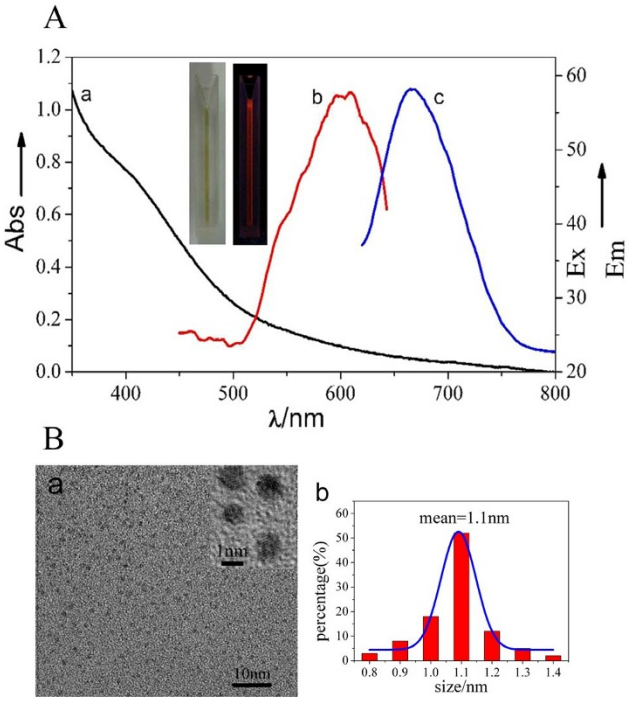

Figure 1 | (A) Optical microscopy characterization of silver nanoclusters biosynthesized in situ by HeLa cells 24 h after their incubation with $[Ag(GSH)]^+$, 160 μg/mL. Curve a: UV-Vis absorption spectrum of the relevant silver nanoclusters; curve b: excitation spectrum; curve c: fluorescence emission spectrum (Em), with excitation wavelength at 590-nm. Inset: pictures of biosynthesized Ag nanocluster solution under room light (left) and excitation source (right) irradiations. (B) Characterization of the silver nanoclusters biosynthesized in situ by HeLa cells after incubation for 24 h or 48 h with $[Ag(GSH)]^+$. (a) TEM image of biosynthesized silver nanoclusters, evidencing the ~0.1 nm interplanar spacing of the silver nanoclusters (inset). (b) Hydrodynamic diameter measured using DLS (mean value ca. 1.1 nm).

into Ag clusters occurs through the involvement of self-assembling reducing ligand(s), which leads to simultaneously facilitate the reduction course by Ag(0) coordination (viz., decreasing the reduction potential of Ag^+ by decreasing the thermodynamic requirement through stabilizing Ag(0) clusters and facilitating kinetics by avoiding that the reaction proceeds through naked Ag(0) atoms) and effectively tailor the surface of growing Ag NCs. Hence, although this cannot be unambiguously established by the above observations, GSH appears to be the main candidate to play this role in cells owing to its known properties as one of the main intracellular reducing agents and considering the remarkable ability of GSH and GSSG to attach covalently onto silver surfaces and cap silver NCs, as well as because of high concentrations of GSH in cancer cells[21], Note that the reduction of silver ions is highly dependent on the structure of the silver(0) material formed (size, support, etc.). On the other hand, even if GSH is one of the main reducing agents in cells its redox reactions appear to be kinetically limited in chemical solutions, i.e., when they are not catalyzed by the glutathione S-transferase enzymes which are present in cytosol, microsomes, and mitochondria of living cells. Hence it is reasonable to consider that inside cells, GSH may play the role of a reducing agent and ligand of the silver nanoparticles formed. Note that in this respect, $[Ag(GSH)]^+$ solutions are prepared as complexes followed by mixing of the silver salt with 0.6 eqs of GSH (see Experimental Section)[22]. Since GSH has two carboxylic functions, one may envision that $[Ag(GSH)]^+$ consists of silver ions coordinated by the carboxylate moieties of GSH molecules (as

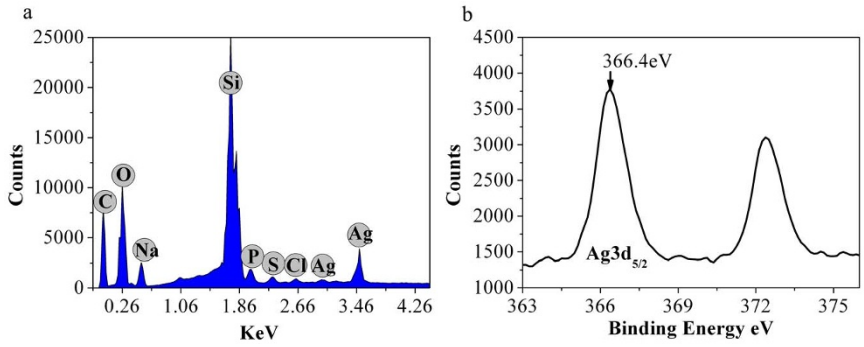

Figure 2 | (a) EDS spectroscopy of the silver nanoclusters biosynthesized in situ by HeLa cells after incubation for 24 h or 48 h with $[Ag(GSH)]^+$. (b) X-ray photoelectron spectra (XPS) evidencing the Ag 3d photo-electron emission from silver nanoclusters biosynthesized in situ by HeLa cells after incubation for 24 h or 48 h with $[Ag(GSH)]^+$.

shown in relevant FTIR spectra of Figure S2), hence it is prone to give readily Ag(0) nuclei coordinated by GSH as soon as they penetrate into cancer cells. EDS result showed that there is no other elemental impurity present in the biosynthesized nanoparticles (Figure 2a). To further confirm the formation of Ag NCs by in situ biosynthesis inside the cells, X-ray photoelectron spectroscopy (XPS) was used to investigate the valence of silver atoms in the Ag NCs after the formation (Figure 2b and Figure 5S). As shown in Figure 2b, two peaks located at the binding energies of 366.4 and 373.6 eV were observed, which is consistent with the emission of 3d photoelectrons from Ag(0), thereby confirming the successful formation of Ag(0) NCs inside HeLa cells[23]. Meanwhile, XPS also evidenced the $S2P_{3/2}$ photo-electron emission from the biosynthesized silver nanoclusters (AgNCs), revealing a binding energy at 163.9 eV, which could be attributed to the formation of disulfide linkage and thus render stability to the cluster [S4–S6] (Figure S5).

Compared cytotoxicity of $AgNO_3$ and $[Ag(GSH)]^+$ in cancer cells by MTT assay. The following was aimed at evaluating possible cytotoxic effects related to the use of the above protocol (viz., self-biosynthesis of Ag NCs from silver salt precursors) in eukaryotic cells. We thus examined the cytotoxic activity of $AgNO_3$ alone or silver complexes (denoted hereafter as $[Ag(GSH)]^+$; see Experimental Section) against cancer cell lines (HeLa, human cervical cancer) or normal cells (L02, normal embryo liver cells) using MTT assays. HeLa cells were seeded in 96-well plates at a density of 5×10^3 cells/well in 0.1 mL of medium and incubated overnight at 37°C in a 5% CO_2 humidified environment. Then different concentrations (10, 40, 70, 100, 130, 160, 190, 220 and 250 μg/mL) of $AgNO_3$ or $[Ag(GSH)]^+$, accordingly, were added into the wells and cells were cultured. In another series of assays, normal embryo liver cells (L02 cells) were treated by $[Ag(GSH)]^+$ and used to compare the effects with those observed with HeLa cells. In all cases the cells were cultured and survival rates were determined after 12, 24, 36, 48 and 72 hours of incubation (compare Figures 3). HeLa cells were easily inhibited by $AgNO_3$, with a 50% inhibiting concentration (IC_{50}) value of 15.5 μg/mL after incubation for 24 h (Figure 3a). Conversely, $[Ag(GSH)]^+$ showed relatively low cytotoxic activity with IC_{50} = 235.6 μg/mL after 24 h incubation time (Figure 3a). In opposition to HeLa cells, L02 normal cells were not significantly affected by the presence of $[Ag(GSH)]^+$ after 24 h of incubation (Figure 3a). It is noted that incubation with the relatively low concentration of $AgNO_3$, i.e., 40 μg/mL of $AgNO_3$, could readily induce rapid HeLa cells death (ca. 12 h half-life time) (Figure 3b). In contrast, in another series of tests HeLa cells survival rates were recorded at 12, 24, 36, 48 and 72 hours after incubation with relevant silver ions concentrations less than the above IC_{50} values, i.e., 130.0 μg/mL of $[Ag(GSH)]^+$, (Figure 3b), incubation with $[Ag(GSH)]^+$ still led to decreased HeLa cells viability but with a half-life time about 6 times longer than that with $AgNO_3$ (Figure 3b). Again, L02 normal cells were not significantly affected since viability remained above ca. 80% after 72 h when incubated with 130.0 μg/mL of $[Ag(GSH)]^+$ (Figure 3b). This is to be paralleled with the fact that treatment of L02 normal cells with $[Ag(GSH)]^+$ did not lead to observable silver NCs intracellular production while after

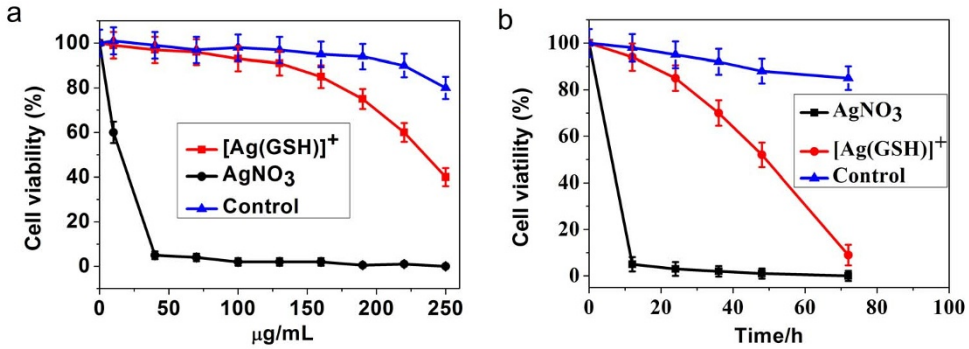

Figure 3 | (a) MTT assay for comparison of cytotoxic activities of $AgNO_3$ and $[Ag(GSH)]^+$ towards HeLa cells and normal ones (L02 cells) treated with $[Ag(GSH)]^+$ and used as control. HeLa cells were treated with $AgNO_3$ or $[Ag(GSH)]^+$ at various concentrations (10, 40, 70, 100, 130, 160, 190, 220, 250 μg/mL) and L02 cells were treated with $[Ag(GSH)]^+$ at various concentrations (10, 40, 70, 100, 130, 160, 190, 220, 250 μg/mL) for 24 h, and cytotoxicity was determined by the MTT method. (b) MTT assay assessment of time-dependent cytotoxicity towards HeLa cells and controls (L02 cells). HeLa cells were treated with $AgNO_3$ (40 μg/mL) or $[Ag(GSH)]^+$ (130 μg/mL) and L02 cells were treated with $[Ag(GSH)]^+$ (130 μg/mL) for different incubation times (12, 24, 36, 48 and 72 hours). Fluorescence excitation wavelength is 590 nm. Data were expressed as the means ± SD (standard deviation) from at least three independent experiments.

24 h a significant amount of biosynthesized Ag NCs was already present in HeLa cells (see Figure S1 and below).

Confocal fluorescence microscopic studies in HeLa cells. Confocal fluorescence microscopy (Leica TCS SP2) measurements at an excitation wavelength of 590 nm were used to assess the method potential for bio-imaging of cancer cells treated with $[Ag(GSH)]^+$. Thus, HeLa cell cultures were incubated with 40 or 100 μg/mL $[Ag(GSH)]^+$ following the above protocol. For control experiments, DMEM (high glucose) medium was used instead of silver ions. After 24 or 48 h, both freshly prepared cell cultures were dropped on rigorously cleaned glass plates and immediately examined by confocal fluorescence microscopy. As expected, no detectable fluorescence signal was observed in control samples treated with DMEM/high glucose medium (Figure 4a). Conversely, intracellular NIR fluorescence (NIRF) was already clearly observable after incubation for 24 h with 40 or 100 μg/mL $[Ag(GSH)]^+$ (Figure 4b and c), although bright-field observation indicated that HeLa cells were viable throughout the imaging study. Similar results were obtained when HepG2 (human hepatocarcinoma cell line) and A549 cells (human alveolar basal epithelial cell line) which were incubated under identical conditions with 100 μg/mL $[Ag(GSH)]^+$ (see Figures S3a and b). On the other hand, comparatively very weak NIRF signals could be observed when the various concentrations of $[Ag(GSH)]^+$ were added to the L02 non-cancerous cells culture (Figure S1), indicating that these non-cancerous cells could not reduce Ag^+ into Ag NCs at a sufficient rate over the range of time considered (24 and 48 h). These series of experiments soundly established that $[Ag(GSH)]^+$ spontaneously evolved to Ag NCs in cancer cells although this could not occur in non-cancerous cell[13,24,25], thus allowing kinetically-controlled selective imaging by NIR fluorescence microscopy.

The above studies performed on cell cultures have evidenced that incubation of cancerous cells (HeLa model) and non-cancerous ones (L02 model) with $[Ag(GSH)]^+$ led to drastic differences concerning (i) the kinetic ability of each cell type to evolve fluorescent silver NCs in their cytoplasms, and (ii) the final outcome in terms of toxicity, which appears somewhat linked to the self-generation of large quantities of Ag NCs by the cells. However, in contrast with usual (viz., chemically synthesized Ag NCs or molecular NIR probes) bio-imaging or active strategies involving fluorophores, the present discrimination relies on different kinetics of silver ions reduction into Ag NCs inside cells according to their redox status so that it does not require any specific targeting by ligand recognition. This is not a serious problem for bio-imaging of cell samples as was shown above but may gravely hamper any use of the present method for *in vivo* imaging of tumors.

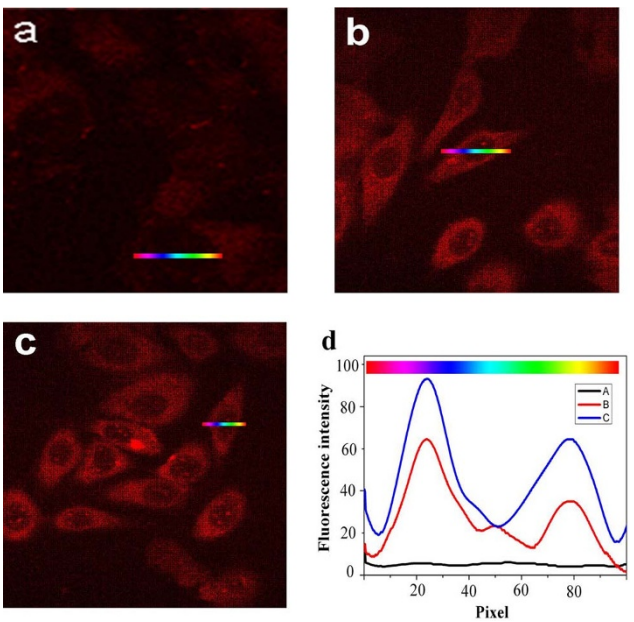

Figure 4 | Effect of different concentrations of $[Ag(GSH)]^+$ on the intracellular accumulation of Ag NCs in HeLa cells. HeLa cells were incubated with DMEM in the absence (a; control) or in the presence of $[Ag(GSH)]^+$ 40.0 μg/mL (b) or 100.0 μg/mL (c) for 24 h at 37°C. The cells were examined under a confocal fluorescence microscope, using a 590 nm fluorescence excitation wavelength. Relative fluorescence intensity variations (d) along cross-sections A (in a), B (in b), or C (in c) (the color gradient coding illustrates the direction of the sampling).

***In vivo* NIR-fluorescent tumor imaging through biosynthesized Ag NCs.** Thus we now wish to explore the possible use of in vivo tumor imaging in situ through spontaneous and discriminative biosynthesis of NIR-fluorescent Ag NCs by living animal tumors. For this, we relied on a xenografted tumor mouse model and examined the possibility of fluorescence detection of subcutaneously xenografted tumors through local injection in the tumors or intravenous treatment of the whole animal with $[Ag(GSH)]^+$. Sixteen nude mice were assigned randomly to four groups consisting of four mice each. Xenografted tumor mouse models of Cervical carcinoma were initially prepared, and $[Ag(GSH)]^+$ complex solution was injected after a few hours either intravenously through the mice tails or directly into the solid tumor. After incubation for a few hours, the tumor was easily spotted and its contour precisely identified under the skin cover by NIR fluorescence at 670 nm (excitation wavelength: 590 nm) regardless of the injection procedure. This indicated that cancer cells had reduced silver ions into silver nanoclusters while this did not occur inside non-cancerous tissues (Figure 5, Figure S4).

Treated mice were dissected after 24 h for ex vivo analysis of the tumor tissue and other organs. The ex vivo observation of the excised tumors closely correlated with the in vivo imaging, confirming that the tumor tissues were highly fluorescent, while no significant fluorescence signal arose from surrounding tissues or from visceral organs like liver, spleen, kidney, etc. (Figure S4). This established definitively that even if these normal tissues were submitted to the $[Ag(GSH)]^+$ solution treatment no Ag NCs evolved inside them as observed on cells cultures.

The high interest of this experimental protocol for therapeutic purposes is also demonstrated by the fact that 7 days after the subcutaneous or intravenous injection of $[Ag(GSH)]^+$ the xenografted tumors decreased in size/volume and gradually disappeared (Figure 5). The relevant body weight has little or almost no change for the mice after treated by $[Ag(GSH)]^+$; However, for the no treated group the mice body weight dramatically decreased, accompanied with significant increase of the tumor size. After 14 days, all the mice treated with $[Ag(GSH)]^+$ were in good health condition, while the mice from the negative control groups were very emaciated or had passed away during this period. Moreover, the histopathological analysis of H&E-stained tissue sections obtained from the harvested organs (i.e., liver, kidney and others) of the xenografted tumor mice after the subcutaneous or intravenous injection of $[Ag(GSH)]^+$ indicated that no histopathological abnormities or lesions were observed in the relevant organs (Data not shown). Furthermore, there were almost no changes in eating, drinking, exploratory behavior, activity, physical features, and neurological status observed in the related tumor-bearing mice or normal mice injected with $[Ag(GSH)]^+$.

Discussion

As described in the above observations, this work has evidenced the high biomedical potential for fast, highly sensitive and specific bio-imaging of tumor cells both under ex vivo (cell cultures) and in vivo

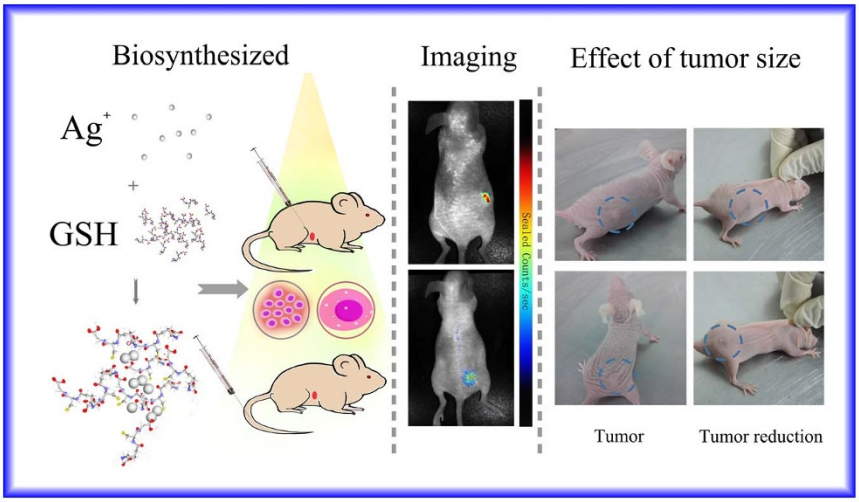

Figure 5 | Representative xenograft tumor nude mice models of Cervical carcinoma observed in normal light (indicating tumor size). The $[Ag(GSH)]^+$ complex solution was administered into the solid tumor mouse model through local injection or intravenous injection through the tail. After incubation for 24 h, fluorescent silver nanoclusters were observed inside the tumors by in vivo fluorescence imaging using a 590 nm excitation wavelength. After 7 days the corresponding tumor was reduced in size and eventually disappeared. In comparison, the negative control groups, which received an equivalent volume of Phosphate Buffered Saline (PBS), did not exhibit any apparent fluorescence. (This figure was prepared by using open source software of Photoshop. The left panel is a cartoon illustration drawn by co-authors for the relevant experimental procedure, including the complexes of Ag^+ with GSH and then biosynthesized to Ag NCs for *in vivo* bio-imaging study, while the middle and right panel is the experimental observations for *in vivo* tumor bio-images, where the $[Ag(GSH)]^+$ complex solution was administered into the solid tumor mouse model through local injection or intravenous injection through the tail.).

(xenografted tumor in nude mice) conditions. This was possible because cancer cells are spontaneously able to rapidly biosynthesize near-infrared-fluorescent Ag NCs when submitted to a $[Ag(GSH)]^+$ treatment while this did not occur as fast in normal cells and tissues. This validates a novel strategy for effective, specific and accurate imaging of cancer cells or tissues by NIR fluorescence based on kinetic differentiation rather than on molecular recognition by specific ligands attached to a fluorophore as is generally performed. Furthermore, $[Ag(GSH)]^+$ treatment did not alter normal tissues or visceral organs in xenografted nude mice. The persistence of Ag NCs biosynthesized inside tumors over several days (7–14) led to a significant decrease in tumor sizes and possibly complete remission. These latter observations stressed that, besides the great interest of the method for rapid and specific bio-imaging of tumors based on readily available simple reagents (modified Tollens procedure and GSH), it also presents a valuable potential interest for treating cancer tissues without significant damage to non-cancer tissues. This is currently being investigated more deeply to optimize the strategy and evaluate its possible long-term effects.

Methods

***In vitro* biosynthesis of Ag NCs in cells.** 1 mL of a 34 μg/mL aqueous solution of silver nitrate ($AgNO_3$) was freshly prepared and used for the biosynthesis of Ag NCs. 1 mL of a 38 μg/mL (0.6 eqs) aqueous solution of GSH (glutathione, (2S)-2-amino-4-{[(1R)-1-[(carboxymethyl)carbamoyl]-2 sulfanylethyl]-carbamoyl}but-anoic acid) was added dropwise into 1 mL 34 μg/mL of aqueous solution of silver nitrate and let to react with silver ions until it became clear. The bulky molecular structure of GSH as the ligand could play a critical role in the gelation with Ag^+ ions, leading to the formation of the relevant stable hydrogel complex. The zeta potential measurements demonstrate that the apparent zeta potential value of the relevant Ag(GSH) complex is $+16.5 \pm 0.8$ mV, thus the complex is denoted as $[Ag(GSH)]^+$ in the text for simplification. The complex mixture was incubated with different cell lines including cancer cells like HepG2 cells, Lung cancers A549 and HeLa cells under culturing conditions.

Characterization of in situ biosynthesized Ag NCs. Silver nanoclusters were biosynthesized *in situ* through incubation of HeLa cells or Lung cancers A549 of a whole culture flask incubated with $[Ag(GSH)]^+$ solution for 24 or 48 h at 37°C, 5% CO_2. Then the presence of biosynthesized Ag NCs was characterized by UV-Vis-NIR, fluorescence spectroscopy, scanning electron microscopy (SEM) and transmission electron microscope (TEM). No formation of silver nanoclusters was observed in L02 control cells incubated with the same protocols.

UV-Vis absorption and fluorescence spectra were also measured from Ag NCs solutions extracted from incubated cancer cells by a repetitive freeze-thaw method, using a UV-Vis-NIR spectrophotometer (Shimadzu, UV3600), and a fluorescence spectrometer (PerkinElmer, LS-55), respectively. The particle size distributions using Dynamic Light Scattering and zeta potential was measured by using a Zetasizer NanoZS size analyzer (ZS90, Malvern, UK). SEM images of the cells interspersed with Ag NCs immobilized on an indium-tin oxide (ITO) glass substrate were taken on a field-emission scanning electron microscope (Zeiss, Ultra Plus). A JEM-2100 transmission electron microscope (TEM) was used to characterize the size and size distribution of *in situ* biosynthesized Ag NCs, which were obtained from the cells by a repetitive freeze-thaw method. The valence state of silver atoms in the *in situ* biosynthesis Ag NCs was investigated by a PHI 5000 VersaProbe X-ray photoelectron spectrometer.

Comparison of cytotoxicities of $AgNO_3$ and $[Ag(GSH)]^+$ in cancer cells by MTT assay. After HeLa cells were treated with different concentrations of $AgNO_3$ or $[Ag(GSH)]^+$, 20 μL of 3-(4,5)-dimethylthiahiazo(-z-y1)-3,5-di-phenytetrazoliumromide (MTT) solution was added to each well and the cells were cultured for 4 hours at 37°C. Thereafter, 150 μL of dimethyl sulfoxide were added to each well to dissolve the formazan crystals using an automated shaker to stir the cells slightly for 10 min. Absorbance of the suspensions was measured by optical density (OD) at a wavelength of 492 nm. Each experiment was repeated at least three times. The cell viability was then expressed as follows: cell viability (%) = [A]test/[A]control × 100%, where [A] represents the absorbance value at 492 nm.

Data were expressed as the means ± SD (standard deviation) from at least three independent experiments. One-tailed unpaired Student's t-test was used for significance testing, and $p < 0.05$ was considered significant.

Construction of the xenografted tumor mouse model. BALB/c female athymic nude mice, age-matched (four weeks of age) and weight-matched (18–22 g), were purchased from Peking University Health Science Center. All experiments involving mice were approved by the National Institute of Biological Science and Animal Care Research Advisory Committee of Southeast University, and experiments were conducted following the guidelines of the Animal Research Ethics Board of Southeast University. The mice were randomly assigned to groups for experimental purposes. They were maintained in clean facilities with a 12-hour light/dark cycle and received water and food through a semi-barrier system. Subcutaneous tumor models were generated by the subcutaneous inoculation (0.10 mL volume containing 5×10^7 cells/mL media) of Hela cells in the right side of their abdomen using a 1-mL syringe with a 25 G needle. Tumor growth was monitored until a palpable size of about 1.0 cm was reached in all directions.

***In-situ* and *in vivo* bio-imaging study.** For cellular imaging, HeLa cells were treated with different concentrations of $AgNO_3$ or $[Ag(GSH)]^+$ solutions and incubated at

37°C for 12, 24 or 48 h. The cells were washed three times with PBS before fluorescence imaging. A 590-nm excitation laser beam (Andor Revolution XD) was focused using a 20 × IR coated objective (Nikon).

For *in vivo* bio-imaging of Ag NCs in the tumor location, the xenograft tumor mice received an administration of 10 mmol/L $[Ag(GSH)]^+$ complex solution (100 μL) *via* tail vein injection. The mice were fully anesthetized by inhalation of a mixture of oxygen with 5% isoflurane at different times post-injection. The *in vivo* bio-images were acquired on Cri Maestro *in vivo* imaging system (excitation: ~590 nm, emission: 700–780 nm). The ROI (regions of interest) analysis was measured under the assistance of CRi Maestro Image software. The studies were approved by the National Institute of Biological Science and Animal Care Research Advisory Committee of Southeast University, while experiments conducted following the guidelines of the Animal Research Ethics Board of Southeast University.

1. Weissleder, R. Scaling down imaging: Molecular mapping of cancer in mice. *Nat Rev Cancer* **2**, 11–18 (2002).
2. Wang, Y. L., Chen, J. J. & Irudayaraj, J. Nuclear Targeting Dynamics of Gold Nanoclusters for Enhanced Therapy of HER2(+) Breast Cancer. *Acs Nano* **5**, 9718–9725 (2011).
3. Yhee, J. Y. *et al.* Optical Imaging of Cancer-Related Proteases Using Near-Infrared Fluorescence Matrix Metalloproteinase-Sensitive and Cathepsin B-Sensitive Probes. *Theranostics* **2**, 179–189 (2012).
4. Choi, H. S. *et al.* Targeted zwitterionic near-infrared fluorophores for improved optical imaging. *Nat Biotechnol* **31**, 148–153 (2013).
5. Mahmood, U., Tung, C. H., Bogdanov, A. & Weissleder, R. Near-infrared optical imaging of protease activity for tumor detection. *Radiology* **213**, 866–870 (1999).
6. Park, H. & Crozier, K. B. Multispectral imaging with vertical silicon nanowires. *Sci. Rep.* **3**, 2460; DOI:10.1038/srep02460 (2013).
7. Saito, K. *et al.* Luminescent proteins for high-speed single-cell and whole-body imaging. *Nat Commun* **3**, 2248 (2012).
8. Dedecker, P., De Schryver, F. C. & Hofkens, J. Fluorescent Proteins: Shine on, You Crazy Diamond. *J Am Chem Soc* **135**, 2387–2402 (2013).
9. Ooyama, H. E. *et al.* Photophysical properties and photostability of novel symmetric polycyclicphenazine-type fluorescent dyes and the dye-doped films. *Dyes Pigments* **94**, 103–112 (2012).
10. Shen, D. W. *et al.* Dual fluorescent molecular substrates selectively report the activation, sustainability and reversibility of cellular PKB/Akt activity. *Sci. Rep.* **3**, 1697; DOI:10.1038/srep01697 (2013).
11. Mazumder, S., Dey, R., Mitra, M. K., Mukherjee, S. & Das, G. C. Review: Biofunctionalized Quantum Dots in Biology and Medicine. *J Nanomater* (2009).
12. Pansare, V. J., Hejazi, S., Faenza, W. J. & Prud'homme, R. K. Review of Long-Wavelength Optical and NIR Imaging Materials: Contrast Agents, Fluorophores, and Multifunctional Nano Carriers. *Chem Mater* **24**, 812–827 (2012).
13. Wang, X., Zhuang, J., Peng, Q. & Li, Y. A general strategy for nanocrystal synthesis. *Nature* **437**, 121–124 (2005).
14. Royon, A. *et al.* Silver Clusters Embedded in Glass as a Perennial High Capacity Optical Recording Medium. *Adv Mater* **22**, 5282–5286 (2010).
15. Wang, C. S. *et al.* Gold Nanoclusters and Graphene Nanocomposites for Drug Delivery and Imaging of Cancer Cells. *Angew Chem Int Edit* **50**, 11644–11648 (2011).
16. Wang, J. *et al.* In vivo self-bio-imaging of tumors through in situ biosynthesized fluorescent gold nanoclusters. *Sci. Rep.* **3**, 1157; DOI:10.1038/srep01157 (2013).
17. Chen, H. M., Zhen, Z. P., Todd, T., Chu, P. K. & Xie, J. Nanoparticles for improving cancer diagnosis. *Mat Sci Eng R* **74**, 35–69 (2013).
18. Xu, H. X. & Suslick, K. S. Water-Soluble Fluorescent Silver Nanoclusters. *Adv Mater* **22**, 1078–1082 (2010).
19. Ueno, T. & Nagano, T. Fluorescent probes for sensing and imaging. *Nat Methods* **8**, 642–645 (2011).
20. Piao, M. J. *et al.* Silver nanoparticles induce oxidative cell damage in human liver cells through inhibition of reduced glutathione and induction of mitochondria-involved apoptosis. *Toxicol Lett* **201**, 92–100 (2011).
21. Zayats, M., Baron, R., Popov, I. & Willner, I. Biocatalytic growth of Au nanoparticles: From mechanistic aspects to biosensors design. *Nano Lett* **5**, 21–25 (2005).
22. Harb, M. *et al.* Optical absorption of small silver clusters: Ag(n), (n = 4–22). *J Chem Phys* **129** (2008).
23. Zhou, T. Y., Rong, M. C., Cai, Z. M., Yang, C. Y. J. & Chen, X. Sonochemical synthesis of highly fluorescent glutathione-stabilized Ag nanoclusters and S2-sensing. *Nanoscale* **4**, 4103–4106 (2012).
24. Manivasagan, P., Venkatesan, J., Senthilkumar, K., Sivakumar, K. & Kim, S. K. Biosynthesis, Antimicrobial and Cytotoxic Effect of Silver Nanoparticles Using a Novel Nocardiopsis sp MBRC-1. *Biomed Res Int* (2013).
25. Riskin, M. *et al.* Switchable surface properties through the electrochemical or biocatalytic generation of Ag-0 nanoclusters on monolayer-functionalized electrodes. *J Am Chem Soc* **128**, 1253–1260 (2006).

Acknowledgments

This work is supported by the National Basic Research Program (2010CB732404) and National Natural Science Foundation of China (81325011, 21175020, 90713023), the National High Technology Research and Development Program of China (863 Program)(No.2012AA022703)In Paris this project is supported by UMR 8640 (ENS-CNRS-UPMC).

Author contributions

S.P.G., C.A. and X.M.W. co-wrote the paper, conducted theoretical analysis, and conceived and designed the experiments. S.P.G., Q.W.L. and H.J. performed the experiments and analyzed the data. S.P.G., Y.J. and D.H.C. were involved in part of the construction of the xenograft tumor mouse model. Q.W.L. and S.P.G. prepared images in relevant figures. All authors contributed to the scientific discussion and revision of the article.

Additional information

Supplementary information accompanies this paper at http://www.nature.com/scientificreports

Competing financial interests: The authors declare no competing financial interests.

How to cite this article: Gao, S.P. *et al.* Near-infrared fluorescence imaging of cancer cells and tumors through specific biosynthesis of silver nanoclusters. *Sci. Rep.* **4**, 4384; DOI:10.1038/srep04384 (2014).